Available online at www.sciencedirect.com
ScienceDirect
Journal of Sound and Vibration 298 (2006) 1099–1112
JOURNAL OF SOUND AND VIBRATION
www.elsevier.com/locate/jsvi

Modelling localised nonlinearities using the harmonic nonlinear super model

Primož Čermelj, Miha Boltežar*

University of Ljubljana, Faculty of Mechanical Engineering, Aškerčeva 6, 1000 Ljubljana, SI Slovenia

Received 23 June 2005; received in revised form 13 June 2006; accepted 15 June 2006
Available online 17 August 2006

Abstract

This paper presents an approximate, frequency-domain approach to modelling complex structures (CSs) with localised nonlinearities, designated here as complex sub-systems. This consistent approach to modelling CSs presented here aims to improve the computational efficiency, which in cases when nonlinearities are included, is a major problem when CSs with many degrees of freedom are modelled. This approach proposes sub-structuring of the CS into its linear and nonlinear parts in the first stage. Classical reduction of the linear part and the nonlinear model reduction and the polynomial approximation for the nonlinear part are employed in the second stage to decrease the overall number of degrees of freedom. Finally, an additional, well-suited harmonic-balance and describing-function-based approximation is used for the nonlinear part, introducing the *multi-coordinate describing functions* (MCDFs) and the *multi-coordinate describing-function matrix* (MCDFM). Together with the matrices of the linear part of the localised nonlinearity, the MCDFM forms the so-called *harmonic nonlinear super-model* (HNSM). The HNSM introduced is well-suited for use with FRF coupling in the frequency domain. Two numerical case studies as well as an experimental case study showed that this approach is suitable for the steady-state vibration of CSs with localised nonlinearities, while at the same time, the efficient approach makes it possible to perform parametric analyses. It is shown that, with some restrictions, an optional reconstruction is also possible, which makes this approach even more efficient.

1. Introduction

In structural dynamics, complex structures (CSs) are structures whose models usually have many degrees of freedom (dofs) and also, on occasions, complex sub-systems (CSSs), which are in general nonlinear. CSSs, therefore, represent localised nonlinearities. In order for them to be suitable for solving numerically, overall models of CSs, e.g., electro-motors, washing machines, suction-units, engines, etc., usually need to be simplified using either linear models instead of nonlinear ones, using reduction, or some alternative approaches to solving the problem. Ewins and Inman [1], and Dascotte and Swindell [2] stated that there is the following tendency in the modelling of structures: "*The model should be as simple as possible while still reflecting the most significant properties*". In terms of the number of dofs, the models should be smaller, not

*Corresponding author. Tel.: +386 1 4771 608; fax: +386 1 2518 567.
E-mail address: miha.boltezar@fs.uni-lj.si (M. Boltežar).

0022-460X/$ - see front matter
doi:10.1016/j.jsv.2006.06.042

bigger. This rule is especially true for nonlinear structures, CSSs in our case, whose models are mostly either models with equivalent linear parameters obtained using updating, e.g. Refs. [3–6], or, on the other hand, models where a certain nonlinearity is investigated in a detailed way, but with simplified models of the surrounding structure, e.g. Ref. [7]. But, in cases when a certain CSS is represented by an equivalent, linear model, the nonlinear effects cannot be included in the overall model of the CS, while the linear-model parameters are operating-point-dependent. The cost- and time-expensive updating of the CSS's nonlinear properties is required is such cases. On the other hand, with respect to numerical solving capabilities, one cannot afford to include detailed models of CSSs into the model of the CS.

While the exact, time-domain methods of direct integration are usually not suitable for simulating the dynamics of CSs, a frequency-domain approach can be used as an efficient counterpart if the assumption of a steady-state condition holds, which is reasonable for many engineering problems. In such cases, the principles of harmonic balance or a describing function are usually employed, but the nonlinear part of the whole structure, CSSs, are usually modelled as systems with parallel springs, as the most simple systems, which are especially suitable for harmonic-balance-based approaches [8–11]. Although they are nonlinear, these "parallel springs" [8–13] do not usually have a meaningful physical connection with real sub-systems, like bearings, bolted joints, weld-spots, etc., so their properties cannot be derived directly; instead, again, some kind of updating or identification is in general required.

To partially overcome the limitations in modelling CSSs just mentioned, especially the need for updating, our goal in this paper is to present a new, frequency-domain approach to building simple but still nonlinear super-models of CSSs that can be easily incorporated into the overall CS model and, eventually, be suitable for efficient numerical analyses, even in the parametric sense. Here the focus will be on the determination of the stiffness nonlinearity while the mass and damping of a CSS are known a priori or can be easily determined. To present the main idea behind this approach, the generation of a detailed nonlinear model of a certain CSS, e.g., a finite-element-based model, which is further reduced and approximated in order to derive a simple but still valid CSS model for the use with the coupling in the frequency domain, this paper is organized as follows: Section 2 presents the new approach, the generation of the harmonic nonlinear super-model (HNSM) as well as its incorporation to the overall, linear structure, Section 3 describes the approach to solving of the overall, nonlinear response the CS and with the optional reconstruction, Section 4 shows three numerical case studies to show the usability of the proposed approach while Section 5 describes the procedure and results of the experimental validation of the approach which are also summarized in the conclusions.

2. HNSM

Following the idea mentioned in the preceding section, the problem of modelling CSs in the frequency domain can be schematically depicted as in Fig. 1. The approach shown in Fig. 1 starts with detailed models of both the linear part (LS) and the nonlinear part (CSS) of the CS. While the obtaining of valid models for the LS is a well-established field in structural dynamics, e.g. Refs. [1,4], the focus here will be mainly on how to determine the so-called HNSM, assuming a valid model of the LS can be obtained. Working in the frequency domain actually means that one is working with the response models of the CSS and LS parts of the CS, and that FRF coupling techniques [3,9,14] are used to couple these two sub-systems together. For that, the CSS response model needs to be in a form suitable for coupling with the linear part of the CS. Here, the FRF coupling approach from Liu [3,14] will be used that relates the amplitudes of the forcing force $\mathbf{F}$ and the nonlinear response amplitudes $\mathbf{X}$ and was used by Liu for linear systems only. It will be shown that the same approach can be used for coupling the linear and nonlinear response models together. When only the fundamental frequency is considered and when the CSS model has only the connection (c) DOFs, one can write [3,9,14]

$$\begin{pmatrix} \mathbf{X}_I \\ \mathbf{X}_C \end{pmatrix} = \begin{bmatrix} \mathbf{H}_{ii} - \mathbf{H}_{ic}(\mathbf{I} + \mathbf{Z}_{\mathrm{CSS}}\mathbf{H}_{cc})^{-1}\mathbf{Z}_{\mathrm{CSS}}\mathbf{H}_{ci} & \mathbf{H}_{ic}(\mathbf{I} + \mathbf{Z}_{\mathrm{CSS}}\mathbf{H}_{cc})^{-1} \\ \mathbf{H}_{ci} - \mathbf{H}_{cc}(\mathbf{I} + \mathbf{Z}_{\mathrm{CSS}}\mathbf{H}_{cc})^{-1}\mathbf{Z}_{\mathrm{CSS}}\mathbf{H}_{ci} & \mathbf{H}_{cc}(\mathbf{I} + \mathbf{Z}_{\mathrm{CSS}}\mathbf{H}_{cc})^{-1} \end{bmatrix} \begin{pmatrix} \mathbf{F}_I \\ \mathbf{F}_C \end{pmatrix}, \tag{1}$$

where I and C indices designate the internal and coupling dofs of the connected structure and i and c are the internal and coupling coordinates of the de-coupled (collected) structure as defined in Refs. [9,14]. $\mathbf{H}$ are FRF

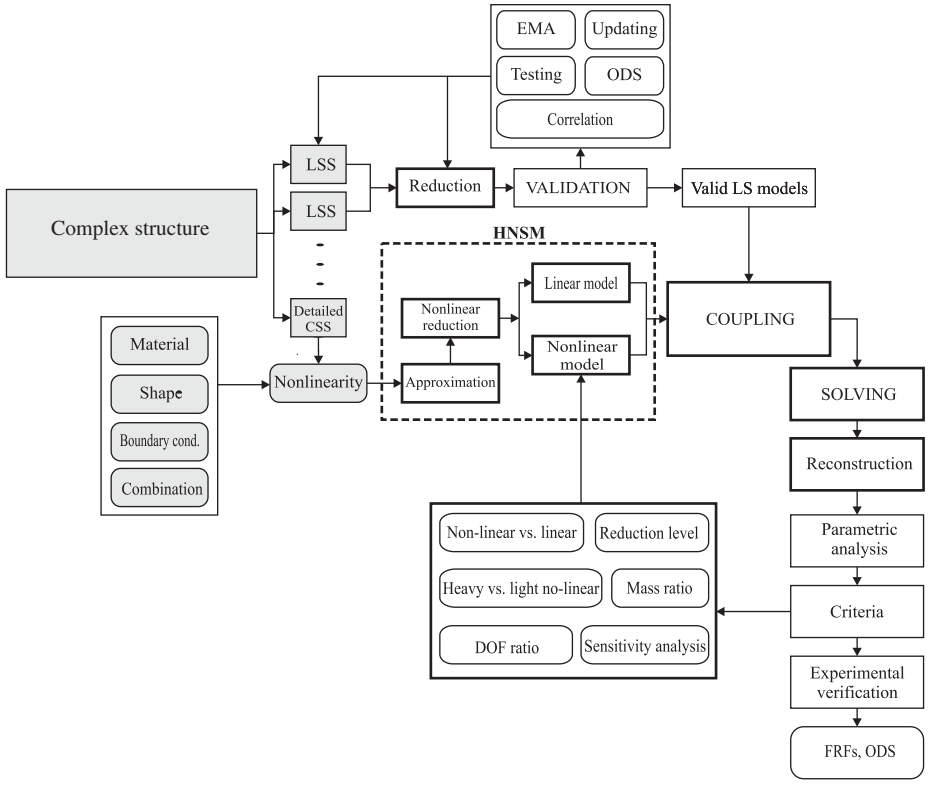

Fig. 1. A consistent approach to solving a CS with localised nonlinearities; suitable for the frequency domain and the steady-state condition.

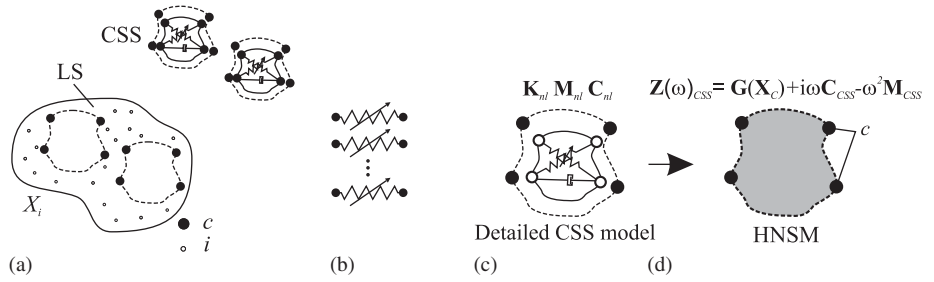

Fig. 2. The complex structure and complex sub-systems (CSSs) de-coupled (a), a schematic representation of the simplest CSSs model—parallel springs (b) and a schematic representation of a detailed CSSs along with the transformation to the reduced, harmonic nonlinear super-model (c).

matrices and $\mathbf{Z}_{CSS}$ represents the *displacement-dependent* nonlinear impedance matrix of the CSS model without internal DOFs while $\mathbf{I}$ is the identity matrix. As $\mathbf{Z}_{CSS}$ is a displacement-dependent impedance matrix, Eq. (1) represents a set of nonlinear algebraic equations that can be solved using the Newton–Raphson approach, for example. Using reduction for the LS and CSS models, and also reconstruction, as will be seen later, Eq. (1) can be solved more efficiently than a system of nonlinear differential equations in the time-domain approaches. Also, the HNSM approach is more general (Fig. 2(b)) than the common approach of using parallel springs (Fig. 2(a)), e.g. Refs. [8–13], whose parameters cannot be determined from a detailed, FE CSS model. In the subsections that follow, the determination of the HNSM will be shown only for cases of symmetric stiffness nonlinearities.

2.1. Nonlinear model reduction and approximation

According to the FRF coupling of the LS and CSS parts of the CS, Eq. (1), the displacement-dependent nonlinear impedance $\mathbf{Z}_{\mathrm{CSS}}$ needs to be built to reflect the relations between the connection coordinates of the CSS model. For that reason, the connection dofs (c), solid circles in Figs. 2(a)–(c) and 3, are also the master dofs of the CSS model. $\mathbf{M}_{\mathrm{nl}}$, $\mathbf{K}_{\mathrm{nl}}$ and $\mathbf{C}_{\mathrm{nl}}$ are nonlinear stiffness, nonlinear mass and nonlinear damping matrices of the detailed CSS, while $\mathbf{Z}(\omega)_{\mathrm{CSS}}$ represents the nonlinear impedance matrix of the CSS model, where $\mathbf{G}(\mathbf{X}_c)_{\mathrm{nl}}$ is the nonlinear stiffness part of the $\mathbf{Z}_{\mathrm{CSS}}$, while $\mathbf{M}_{\mathrm{CSS}}$ and $\mathbf{C}_{\mathrm{CSS}}$ are linear matrices of the CSS. A CSS model described by $\mathbf{Z}(\omega)_{\mathrm{CSS}}$ is the HNSM.

Moreover, as our approach is to be used for models in the form of localised stiffness nonlinearities, the mass of the CSS can simply be a lumped representation with respect to the master dofs and can easily be determined while the damping can be simply artificially added, identified or even neglected. Further, having a detailed model of the CSS, the static nonlinear force–displacement relation is known for each dof of the detailed CSS model and, therefore, also for all the retained dofs of the corresponding, reduced HNSM. Assuming a symmetric stiffness nonlinearity and a polynomial approximation with linear and cubic terms, the general, nonlinear force–displacement approximation model for the HNSM could be (for the kth internal force, $\hat{f}_{in_k}$)

$$\hat{f}_{in_k}(\mathbf{x}) = \sum_{j=1}^{n} a_{k_j} x_j + \sum_{j=1}^{n} b_{k_j} x_j^3 + \sum_{j=1}^{n-1} \sum_{i=j+1}^{n} c_{k_j} x_j^2 x_i + \sum_{j=1}^{n-1} \sum_{i=j+1}^{n} d_{k_j} x_j x_i^2 \tag{2}$$

with unknown coefficients a, b, c and d, where x_i is the displacement of the HNSM at ith dof. As the exact force–displacement relation at the retained (master) dofs is known from a detailed CSS model, comparing this model to the model from Eq. (2) in a least-squares sense, the coefficients $\mathbf{p} = \{a_{ij}, b_{ij}, \ldots\}$ from Eq. (2) can be calculated. The random generation of points is a suitable choice when calculating the coefficients $\mathbf{p}$. This procedure corresponds to the *nonlinear model reduction and approximation*, being a simple representation of the CSS, having only a few dofs as well as a simple analytical force–displacement relation. The reason for using the polynomial approximation is because this type of approximation is well suited for use with the describing-function approach.

2.2. Multi-coordinate describing-function matrix

The final phase of building the HNSM is another approximation, the describing-function-based approximation, e.g. Refs. [9–11,13]. This is an equivalent linearization approach and can be used for 1dof systems directly, while in the case of mdof structures, the so-called inter-coordinate notation, $y_{kl} = x_k - x_l$, is usually used; this corresponds to the use of a model of parallel springs [8–13]. In our case a suitable approximation needs to be defined for terms like $a_k x_i^r x_j^q$ from the kth internal force from Eq. (2). Following the basic describing-function approach, e.g. Refs. [9–11], when there is a harmonic forcing function to a nonlinear mdof system, $\mathbf{f}e^{\mathrm{i}\omega t}$, the response at each coordinate is also approximately harmonic, and the same

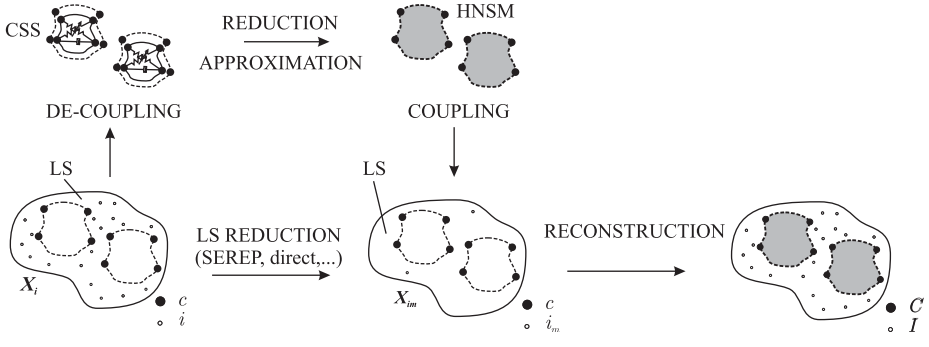

Fig. 3. A schematic view of the overall and efficient process of de-coupling, reduction of the linear (LS) and nonlinear parts (CSS), coupling, and finally, the optional reconstruction of the CS at the end.

applies to each internal force $\hat{f}_{in_k}$ acting on the CSS. In the case of symmetric nonlinearities, only the first term in the truncated, complex Fourier series can be retained, and the responses at some jth and some ith coordinates are then approximated in the form [9–11]

$$x_i \approx X_i e^{i\omega t}, \quad \bar{x}_i = \Im(x_i) = \bar{X}_k \sin(\omega t + \phi_i), \quad X_i \in \mathbb{C}, \ \bar{X}_i \in \mathbb{R},$$

$$x_j \approx X_j e^{i\omega t}, \quad \bar{x}_j = \Im(x_j) = \bar{X}_j \sin(\omega t + \phi_j), \quad X_j \in \mathbb{C}, \ \bar{X}_j \in \mathbb{R} \tag{3}$$

with $\bar{x}_i$ and $\bar{X}_i$ representing the real displacement and magnitude of the response, respectively, at the coordinate i. ϕ_i is the phase shift of the response x_i. Unlike in the case of linear systems, where the principle of superposition holds, the complex notation used here is actually an artificial expansion of real quantities into the complex form; however, only the imaginary part is considered. This way the magnitude and the phase can easily be handled.

It can be shown that inserting Eq. (3) into $a_k x_i^r x_j^q$ does not enable one to find describing functions in a closed form, as in the case of one-coordinate or inter-coordinate terms, so, further imposing the relation $\phi_i \approx \phi_j = \phi_{ij}$ simplifies to

$$\omega t = \tau, \quad \tau + \phi_{ij} = \psi_{ij} \tag{4}$$

with τ as the new time variable and ψ_{ij} as the new variable comprising the frequency and the phase of the response between the coordinates i and j. This enables us to find the Fourier coefficient for the i,j pair of the kth internal force $\hat{f}_k$, $F_{k_{i,j}}$,

$$F_{k_{i,j}} = \frac{i}{\pi} \int_0^{2\pi} \hat{f}_{in_{k_{i,j}}}(\bar{x}_j, \bar{x}_i) e^{-i\psi_{ij}} \, d\psi_{ij}, \tag{5}$$

where

$$a_k x_i^r x_j^q \approx \hat{f}_{in_{k_{i,j}}} = F_{k_{i,j}} e^{i\psi_{ij}} = a_k C \bar{X}_i^r \bar{X}_j^q e^{i\psi_{ij}} \tag{6}$$

with C as an r- and q-dependent constant. Considering the relations

$$\bar{X}_i e^{i\psi_{ij}} = \bar{X}_i e^{i\phi_{ij}} e^{i\tau} = X_i e^{i\tau} = x_i,$$

$$\bar{X}_j e^{i\psi_{ij}} = \bar{X}_j e^{i\phi_{ij}} e^{i\tau} = X_j e^{i\tau} = x_j \tag{7}$$

and artificially expanding the expression from Eq. (6) to a number of terms that correspond to the number of coordinates in the nonlinear term $a_k x_i^r x_j^q$, the following is obtained:

$$\begin{aligned} a_k x_i^r x_j^q &= \tfrac{1}{2} a_k C \bar{X}_i^{r-1} \bar{X}_j^q x_i + \tfrac{1}{2} a_k C \bar{X}_i^r \bar{X}_j^{q-1} x_j \\ &= v^{(i)}(\bar{X}_i, \bar{X}_j) x_i + v^{(j)}(\bar{X}_i, \bar{X}_j) x_j, \end{aligned} \tag{8}$$

where $v^{(i)}$ and $v^{(j)}$ are *multi-coordinate describing functions* (MCDFs) for the term $a_k x_i^r x_j^q$, and what is also evident is that the restriction $\phi_i \approx \phi_j = \phi_{ij}$ is no longer needed. By considering all the MCDFs with respect to the relations from Eq. (2) the *multi-coordinate describing-function matrix* (MCDFM) can be formed, $\mathbf{G}(\bar{\mathbf{X}})$, relating the internal elastic force (linear + nonlinear), $\mathbf{f}_{in}$, and the complex displacement magnitudes, $\mathbf{X}$

$$\hat{\mathbf{f}}_{in} \approx \mathbf{G}(\bar{\mathbf{X}}) \mathbf{X} e^{i\tau}, \quad \mathbf{G}(\bar{\mathbf{X}}) = \mathbf{K}_{lin} + \mathbf{G}_{nl}(\bar{\mathbf{X}}), \quad \mathbf{G}, \mathbf{X} \in \mathbb{C}. \tag{9}$$

$\mathbf{G}(\bar{\mathbf{X}})$ can be, in general, represented by the linear part $\mathbf{K}_{lin}$ and the nonlinear part $\mathbf{G}_{nl}(\bar{\mathbf{X}})$, while together with the mass and damping matrices designates the so-called HNSM, $\mathbf{Z}_{CSS}$

$$\mathbf{Z}_{CSS}(\omega, \bar{\mathbf{X}}) = \mathbf{G}(\bar{\mathbf{X}}) + i\omega \mathbf{C}_{CSS} - \omega^2 \mathbf{M}_{CSS}. \tag{10}$$

The HNSM defined in Eq. (10) is the nonlinear impedance matrix of the CSS that can be used in either the impedance or FRF coupling approach [3,9,14] to couple the CSS with the linear part of the CS.

3. Response determination and reconstruction

The system from Eq. (1) can be written in a more compact form

$$\mathbf{X}_{I,C} = \mathbf{H}_{\mathrm{nl}}(\omega, \mathbf{X}_C)\mathbf{F}_{I,C} \tag{11}$$

with $\mathbf{H}_{\mathrm{nl}}(\omega, \mathbf{X}_C)$ designating the frequency- and magnitude-dependent, nonlinear FRF matrix and with $\mathbf{X}_{I,C}$ and $\mathbf{F}_{I,C}$ as displacement amplitudes and force amplitudes, respectively, partitioned in terms of I and C dofs. The system of nonlinear algebraic equations from Eq. (11) is solved numerically, but to gain in terms of efficiency, the linear part of the CS is usually reduced. All the internal dofs (i, I) can be removed (reduced) except for those where there are external forces and those where the responses are to be calculated. For CSs with many dofs this enables an efficient calculation, especially suitable for parametric analyses.

While the reduction is, in most cases, needed for an efficient calculation or even for the ability to calculate the response of the CS, one can even reconstruct the nonlinear responses at the reduced internal dofs, i.e., if the modal properties of the LS are known and if the CSS model has only the so-called connection dofs, the reduction of the full set of dofs, $\mathbf{X}_{I_N,C}$, can be written with respect to the reduced or master dofs, $\mathbf{X}_{I_n,C}$, e.g. [3,12]

$$\mathbf{X}_{I_N,C} = \mathbf{T}_{i,c}\mathbf{X}_{I_n,C} \tag{12}$$

with the reconstruction matrix $\mathbf{T}_{i,c}$

$$\mathbf{T}_{i,c} = \Phi_{N\times M}\Phi^{+}_{n\times M}. \tag{13}$$

The reconstruction matrix $\mathbf{T}_{i,c}$ contains the modal properties, the modal matrix Φ, of the LS, de-coupled from the CS. M is the number of modal vectors used for the SEREP-based (system equivalent reduction-expansion process, SEREP) reconstruction from Eq. (12), N is the number of all the dofs, while n is the number of master dofs of the LS. For the partial modal matrix $\Phi_{n\times M}$ from Eq. (13) to be unique, the following must hold, e.g. Refs. [3,12]

$$M \leqslant n \;\Rightarrow\; \mathrm{rank}(\Phi_{n\times M}) \geqslant M. \tag{14}$$

This means that one usually has to retain as many internal dofs as there are modes used for the reconstruction. For practical use this number can be relatively low with respect to the full, non-reduced system. Moreover, this relation is also valid in cases when the LS part of the CS is formed of many parts in the de-coupled state, which means that this approach is general and does not require special handling, only for the master–slave partitioning, i.e., the partitioning used in Eq. (1). Fig. 3 shows the overall process of de-coupling the LS and CSS parts from the CS, the reduction of both parts, the creation of the HNSM, the coupling and, finally, the optional reconstruction.

4. Numerical case studies

To verify the proposed methods and the overall approach using the HNSM (see Fig. 1) the two numerical case studies shown in Figs. 4 and 5 were investigated, with both satisfying the equation of nonlinear forced motion under the steady-state condition

$$\mathbf{M}\ddot{\mathbf{x}} + \mathbf{C}\dot{\mathbf{x}} + \mathbf{K}\mathbf{x} + \mathbf{f}_{\mathrm{nl}}(\mathbf{x}) = \mathbf{f}(t) = \mathbf{F}\sin(\omega t) \tag{15}$$

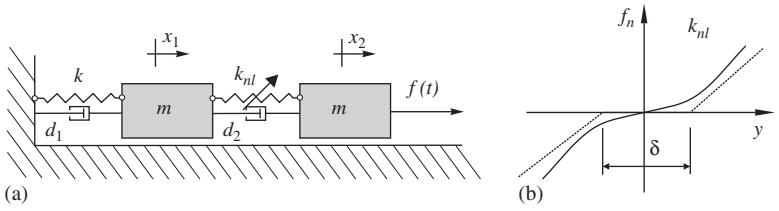

Fig. 4. A 2-dof system with the second spring being nonlinear (a) and with two types of nonlinearities (b), cubic nonlinearity and clearance.

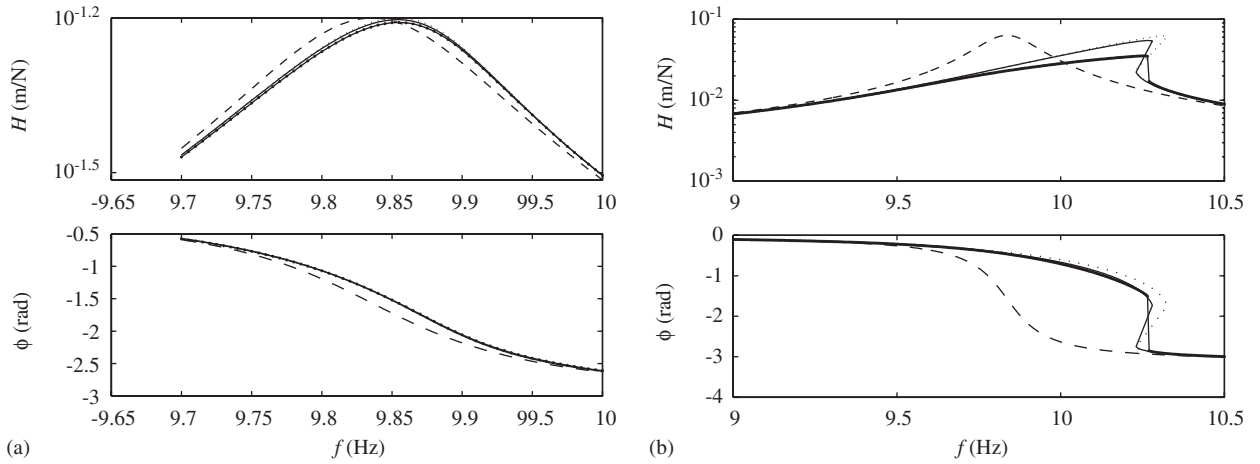

Fig. 5. Three nonlinear, first-order FRFs with the FRF of the underlying linear system from Fig. 4 and for the case of the cubic-hardening stiffness. The amplitude of the forcing harmonic force was 0.5 N (a) and 5 N (b). (- - -) represents the FRF of the underlying linear system; (-.-) represents the nonlinear FRF using the time-domain integration; (...) is the classical describing-function approach; (—) depicts the HNSM approach.

with **M**, **C**, **K** as the linear mass, linear damping and linear stiffness matrices, respectively, with $\mathbf{f}_{\mathrm{nl}}$ as the nonlinear internal force and with **F** as the vector of force amplitudes. These two case studies were chosen as they are simple enough to use the classical parallel-springs approach [8–13], as well as our, the HNSM approach. Another numerical example, the beam structure, was then chosen to demonstrate the usage of the HNSM approach on a structure were the simple parallel-springs-based approach cannot be used and to show the importance of the reduction as well as the importance of the reconstruction.

4.1. 2-dof system

In this case, two types of nonlinearities were considered for the 2-dof system from Fig. 4(a), cubic-hardening stiffness and clearance, Fig. 4(b). In both cases, the mass and damping properties were

$$\mathbf{M} = \begin{bmatrix} m & 0 \\ 0 & m \end{bmatrix}, \quad \mathbf{C} = d\mathbf{K}, \quad \mathbf{F} = (0,\ F_0)^{\mathrm{T}} \tag{16}$$

with d as a factor of proportional, viscous damping and F_0 as an amplitude of the force at the second mass.

4.1.1. Cubic nonlinearity

In the case of the cubic nonlinearity, the underlying stiffness matrix and the exact internal nonlinear force in the second spring were

$$\mathbf{K} = \begin{bmatrix} 2k & -k \\ -k & k \end{bmatrix}, \quad \mathbf{f}_{\mathrm{nl}} = \begin{pmatrix} -k_n(x_2 - x_1)^3 \\ k_n(x_2 - x_1)^3 \end{pmatrix} \tag{17}$$

with k and k_n as two constants for the linear and nonlinear stiffness, respectively. To validate our approach, three approaches are shown for this particular case: the exact approach, using the direct numerical integration, e.g. Ref. [9]; an approach using the inter-coordinate relation [8–13]; and the HNSM approach, presented in this work. In the case of the inter-coordinate relation, the internal nonlinear force can be written with respect to the inter-coordinate displacement y as

$$\mathbf{f}_{\mathrm{nl}} = \begin{pmatrix} -k_n y^3 \\ k_n y^3 \end{pmatrix}, \quad y = x_2 - x_1 \tag{18}$$

and following the classical DF approach with respect to inter-coordinate notation it follows that [8–13]

$$y \approx Y e^{i\tau}, \quad \bar{y} = \Im(y) = \bar{Y}\sin(\tau+\phi), \quad Y = X_2 - X_1, \tag{19}$$

and finally,

$$\mathbf{f}_{nl} \approx \begin{pmatrix} F_1 \\ F_2 \end{pmatrix} e^{i\tau} = \begin{pmatrix} v_1 Y \\ v_2 Y \end{pmatrix} e^{i\tau} = \begin{pmatrix} -k_n \tfrac{3}{4}\bar{Y}^2 \\ k_n \tfrac{3}{4}\bar{Y}^2 \end{pmatrix} (X_2 - X_1) e^{i\tau} \tag{20}$$

which can also be written in the form

$$\mathbf{f}_{nl} \approx \begin{bmatrix} -v_1 & v_1 \\ -v_2 & v_2 \end{bmatrix} \begin{pmatrix} X_1 \\ X_2 \end{pmatrix} e^{i\tau} = \mathbf{G}_{nl}\mathbf{X}e^{i\tau}. \tag{21}$$

This is the classical approach using parallel springs, being useful only for some simple CSSs like in this case.

On the other hand, for the HNSM approach, the following approximation of the internal nonlinear force can be used

$$\hat{\mathbf{f}}_{nl} = \begin{pmatrix} -k_n(-x_1^3 + x_2^3 + 3x_2x_1^2 - 3x_2^2x_1) \\ k_n(-x_1^3 + x_2^3 + 3x_2x_1^2 - 3x_2^2x_1) \end{pmatrix} \tag{22}$$

which, after applying the approach from Section 2, gives the corresponding MCDFM

$$\mathbf{G}_{nl}(\mathbf{X}) = \begin{bmatrix} v_{11} & v_{12} \\ v_{21} & v_{22} \end{bmatrix} = \begin{bmatrix} -k_n(-\frac{3}{4}\bar{X}_1^2 + \frac{9}{8}\bar{X}_1\bar{X}_2 - \frac{9}{8}\bar{X}_2^2) & -k_n(\frac{3}{4}\bar{X}_2^2 + \frac{9}{8}\bar{X}_1^2 - \frac{9}{8}\bar{X}_1\bar{X}_2) \\ k_n(-\frac{3}{4}\bar{X}_1^2 + \frac{9}{8}\bar{X}_1\bar{X}_2 - \frac{9}{8}\bar{X}_2^2) & k_n(\frac{3}{4}\bar{X}_2^2 + \frac{9}{8}\bar{X}_1^2 - \frac{9}{8}\bar{X}_1\bar{X}_2) \end{bmatrix} \tag{23}$$

and thus

$$\hat{\mathbf{f}}_{nl}(x) \approx \mathbf{G}_{nl}\mathbf{X}e^{i\tau}. \tag{24}$$

Fig. 5 compares the three approaches to calculating the so-called first-order nonlinear FRF: the exact approach, using time-domain numerical integration; the DF approach, using inter-coordinate notation; and the HNSM approach, using the MCDFM. It is clear that the proposed HNSM approach is appropriate even when larger nonlinearities are excited (Fig. 5(b)).

4.1.2. Clearance

The same approach can be used for the case of the clearance in the system from Fig. 4(a), but in this case the linear stiffness matrix and the exact internal nonlinear force, respectively, were

$$\mathbf{K} = \begin{bmatrix} k & 0 \\ 0 & 0 \end{bmatrix}, \quad \mathbf{f}_{nl} = \begin{pmatrix} -k(y - \frac{\delta}{2}\operatorname{sgn}(y)) \\ k(y - \frac{\delta}{2}\operatorname{sgn}(y)) \end{pmatrix}, \quad |y| \geqslant 0 \tag{25}$$

while the approximated, total internal force (linear + nonlinear) was chosen first as

$$\hat{\mathbf{f}}_{nl_1} = \begin{pmatrix} a_{11}x_1 + a_{12}x_2 + a_{13}x_1^3 + a_{14}x_2^3 + a_{15}x_1^2x_2 + a_{16}x_1x_2^2 \\ a_{21}x_1 + a_{22}x_2 + a_{23}x_1^3 + a_{24}x_2^3 + a_{25}x_1^2x_2 + a_{26}x_1x_2^2 \end{pmatrix} \tag{26}$$

and then also as

$$\hat{\mathbf{f}}_{nl_2} = \begin{pmatrix} a_{11}x_1^3 + a_{12}x_2^3 + a_{13}x_1^2x_2 + a_{14}x_1x_2^2 \\ a_{21}x_1^3 + a_{22}x_2^3 + a_{23}x_1^2x_2 + a_{24}x_1x_2^2 \end{pmatrix}. \tag{27}$$

It was found that the second form, the form without the linear terms, Eq. (27), is a better approximation for the clearance-type nonlinearity whose MCDFM is

$$\mathbf{G}_{nl} = \begin{bmatrix} \frac{3}{4}a_{11}\bar{X}_1^2 + \frac{3}{8}a_{13}\bar{X}_1\bar{X}_2 + \frac{3}{8}a_{14}\bar{X}_2^2, & \frac{3}{4}a_{12}\bar{X}_2^2 + \frac{3}{8}a_{13}\bar{X}_1^2 + \frac{3}{8}a_{14}\bar{X}_1\bar{X}_2 \\ \frac{3}{4}a_{21}\bar{X}_1^2 + \frac{3}{8}a_{23}\bar{X}_1\bar{X}_2 + \frac{3}{8}a_{24}\bar{X}_2^2, & \frac{3}{4}a_{22}\bar{X}_2^2 + \frac{3}{8}a_{23}\bar{X}_1^2 + \frac{3}{8}a_{24}\bar{X}_1\bar{X}_2 \end{bmatrix}. \tag{28}$$

The exact and approximate total internal forces for the case of the clearance are shown in Fig. 6(a), while in Fig. 6(b) examples of the first-order nonlinear FRFs are shown for the three approaches. Again, it was shown that the HNSM model, though simple, is a proper choice, and using this approach one is able to predict the nonlinear response amplitudes of CSs. To emphasize the importance of the proposed approach, the calculation time for the exact nonlinear FRF from Fig. 6(b) took 7 min, while for all the other approaches the calculation took 20 s.

4.2. Beam structure

In the case of the beam-like structure from Fig. 7 the exact internal nonlinear force was

$$\mathbf{f}_{\mathrm{nl}} = \begin{pmatrix} k_{n_1}(y_1 - y_2)^3 \\ k_{n_2}(\varphi_1 - \varphi_2)^3 \\ -k_{n_1}(y_1 - y_2)^3 \\ -k_{n_2}(\varphi_1 - \varphi_2)^3 \end{pmatrix}, \quad k_{n_1} = 5000\,\frac{EI}{l^3}, \quad k_{n_2} = 200\,\frac{EI}{l^2}, \tag{29}$$

where φ_i is the rotation and y_i is the displacement of the beam's finite element. The underlying linear properties of each of the finite elements, the linear stiffness $\mathbf{K}$ and linear masses $\mathbf{M}$, $\mathbf{M}_{\mathrm{CSS}}$

$$\mathbf{K} = \frac{EI}{l^3}\begin{bmatrix} 12 & 6l & -12 & 6l \\ & 4l^2 & -6l & 2l^2 \\ \text{symm.} & & 12 & -6l \\ & & & 4l^2 \end{bmatrix}, \quad \mathbf{M} = \mathbf{M}_{\mathrm{CSS}} = \frac{\mu l}{420}\begin{bmatrix} 156 & 22l & 54 & -13l \\ & 4l^2 & 13l & -3l^2 \\ \text{symm.} & & 156 & -22l \\ & & & 4l^2 \end{bmatrix}, \tag{30}$$

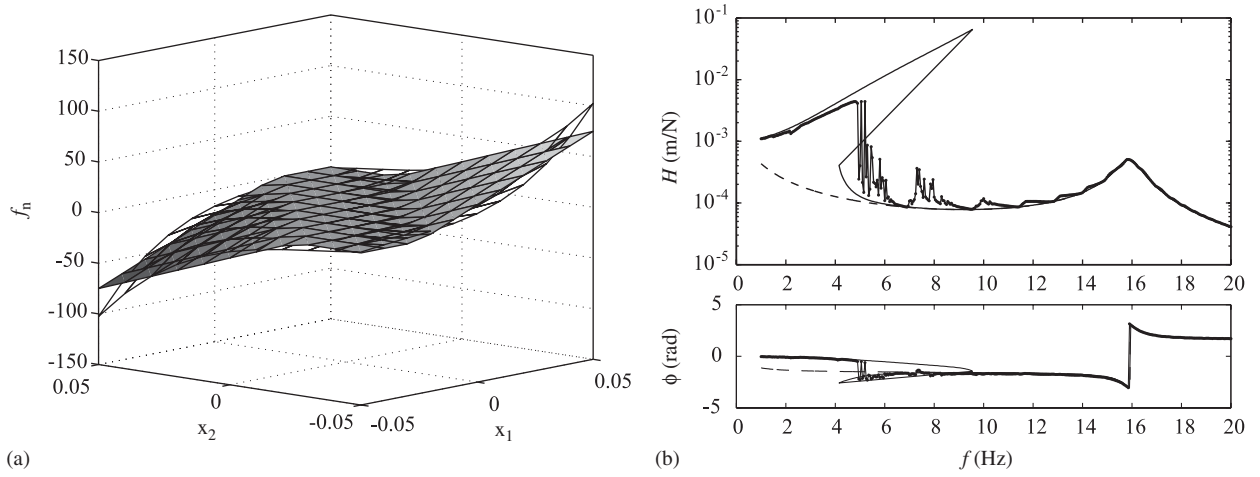

Fig. 6. The exact (filled surface) and the approximate (mesh) internal force for the case of clearance (a) and nonlinear first-order FRFs with the FRF of the underlying linear system (Fig. 4) (b). The amplitude of the forcing harmonic function was 3 N. (- - -) represents the FRF of the underlying linear system; (-.-) represents the nonlinear FRF using the time-domain integration; (—) depicts the HNSM approach.

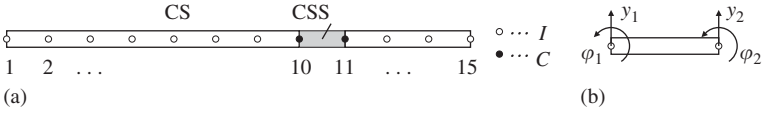

Fig. 7. A CS composed of two linear beams and one nonlinear beam as a CSS (a); the structure is modelled using 4dof finite elements (b).

and the proportional, linear damping for the linear as well as for the nonlinear part

$$\mathbf{C} = 10\mathbf{M}, \quad \mathbf{C}_{\mathrm{CSS}} = 1000\mathbf{M}_{\mathrm{CSS}}. \tag{31}$$

The approximation of the force–deflection relation for the total internal force of the CSS model (linear + nonlinear part), and for the kth component, was assumed to be

$$\begin{aligned}\hat{f}_k = {} & a_{k1}y_1 + a_{k2}\varphi_1 + a_{k3}y_2 + a_{k4}\varphi_2 + a_{k5}y_1^3 + a_{k6}\varphi_1^3 + a_{k7}y_2^3 + a_{k8}\varphi_2^3 \\ & + a_{k9}y_1^2\varphi_1 + a_{k10}y_1\varphi_1^2 + a_{k11}y_1^2y_2 + a_{k12}y_1y_2^2 + a_{k13}y_1^2\varphi_2 + a_{k14}y_1\varphi_2^2 \\ & + a_{k15}\varphi_1^2y_2 + a_{k16}\varphi_1y_2^2 + a_{k17}\varphi_1^2\varphi_2 + a_{k18}\varphi_1\varphi_2^2 + a_{k19}y_2^2\varphi_2 + a_{k20}y_2\varphi_2^2,\end{aligned} \tag{32}$$

resulting in the two matrices representing the HNSM of the nonlinear, 4-dof beam element, the linear and nonlinear part of the HNSM's MCDF

$$\mathbf{K}_{\mathrm{CSS_{lin}}} = \begin{bmatrix} a_{11} & a_{12} & a_{13} & a_{14} \\ a_{21} & a_{22} & a_{23} & a_{24} \\ a_{31} & a_{32} & a_{33} & a_{34} \\ a_{41} & a_{42} & a_{43} & a_{44} \end{bmatrix}, \quad \mathbf{G}_{\mathrm{CSS_{nl}}} = \begin{bmatrix} v_{11} & v_{12} & v_{13} & v_{14} \\ v_{21} & v_{22} & v_{23} & v_{24} \\ v_{31} & v_{32} & v_{33} & v_{34} \\ v_{41} & v_{42} & v_{43} & v_{44} \end{bmatrix}. \tag{33}$$

The MCDFs from Eq. (33) are then (for the kth row)

$$\begin{aligned} v_{k1} &= \tfrac{3}{4}(a_{k5}\bar{Y}_1^2 + \tfrac{1}{2}a_{k9}\bar{Y}_1\bar{\phi}_1 + \tfrac{1}{2}a_{k10}\bar{\phi}_1^2 + \tfrac{1}{2}a_{k11}\bar{Y}_1\bar{Y}_2 + \tfrac{1}{2}a_{k12}\bar{Y}_1^2 + \tfrac{1}{2}a_{k13}\bar{Y}_1\bar{\phi}_2 + \tfrac{1}{2}a_{k14}\bar{\phi}_2^2), \\ v_{k2} &= \tfrac{3}{4}(a_{k6}\bar{\phi}_1^2 + \tfrac{1}{2}a_{k9}\bar{Y}_1^2 + \tfrac{1}{2}a_{k10}\bar{Y}_1\bar{\phi}_1 + \tfrac{1}{2}a_{k15}\bar{\phi}_1\bar{Y}_2 + \tfrac{1}{2}a_{k16}\bar{Y}_2^2 + \tfrac{1}{2}a_{k17}\bar{\phi}_1\bar{\phi}_2 + \tfrac{1}{2}a_{k18}\bar{\phi}_2^2), \\ v_{k3} &= \tfrac{3}{4}(a_{k7}\bar{Y}_2^2 + \tfrac{1}{2}a_{k11}\bar{Y}_1^2 + \tfrac{1}{2}a_{k12}\bar{Y}_1\bar{Y}_2 + \tfrac{1}{2}a_{k15}\bar{\phi}_1^2 + \tfrac{1}{2}a_{k16}\bar{\phi}_1\bar{Y}_2 + \tfrac{1}{2}a_{k19}\bar{Y}_2\bar{\phi}_2 + \tfrac{1}{2}a_{k20}\bar{\phi}_2^2), \\ v_{k4} &= \tfrac{3}{4}(a_{k8}\bar{\phi}_2^2 + \tfrac{1}{2}a_{k13}\bar{Y}_1^2 + \tfrac{1}{2}a_{k14}\bar{Y}_1\bar{\phi}_2 + \tfrac{1}{2}a_{k17}\bar{\phi}_1^2 + \tfrac{1}{2}a_{k18}\bar{\phi}_1\bar{\phi}_2 + \tfrac{1}{2}a_{k19}\bar{Y}_2^2 + \tfrac{1}{2}a_{k20}\bar{Y}_2\bar{\phi}_2) \end{aligned} \tag{34}$$

and the final nonlinear impedance matrix, representing the HNSM of the CSS, was obtained using Eq. (10).

The result of the coupling at different reduction levels, and with the reconstruction, is shown in Fig. 8. At least 14 master dofs are needed (out of 30) for a good reconstruction in this particular case. The number of

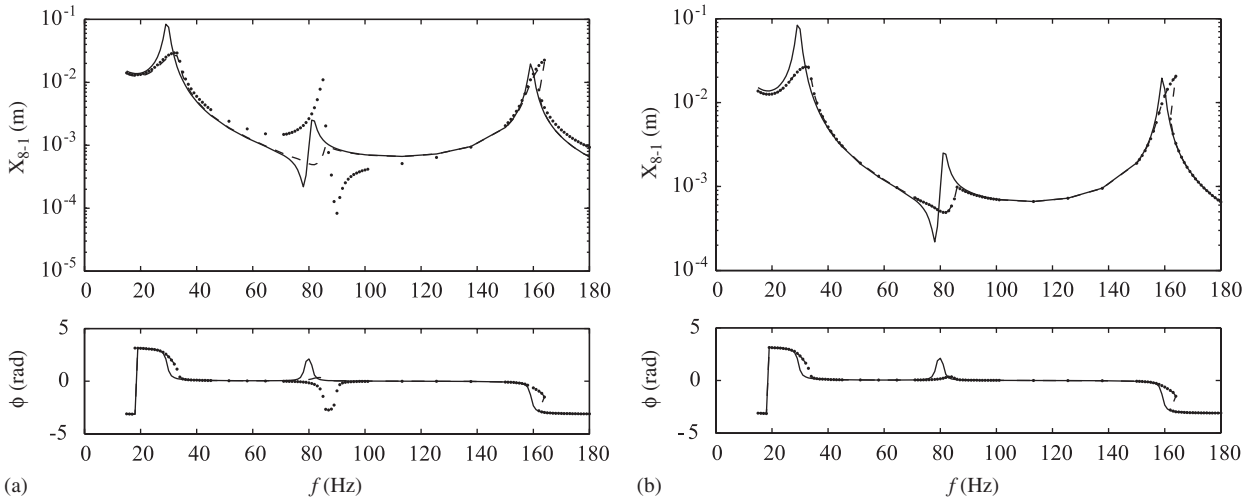

Fig. 8. Nonlinear receptance for the beam from Fig. 7 and the amplitude of the force of 40 N and three different approaches. The node-set retained {1 5 10 11 13 15} (a) does not yield a good result using reconstruction, while retaining one more node (two more dofs) {1 5 8 10 11 13 15} (b) yields a result perfectly correlating with a direct (no reduction) approach. (—) represents the FRF of the underlying linear system; (- - -) represents the nonlinear FRF using the HNSM approach without the reduction; (...) depicts the HNSM approach using the reduction and the reconstruction.

dofs retained in the process of reduction is directly influenced by the number of modes used for the reconstruction, so, in the event that there would be more dofs, the number of master dofs would remain the same. Fig. 9 shows the time needed for a certain number of dofs in the calculation of the nonlinear FRF of the beam. The importance of the reduction is therefore evident.

5. Experimental case study

The special-purpose T-structure shown in Fig. 10 was built [15] in order to verify the proposed approach: the use of the HNSM on a real structure. A very simple structure, composed by two beams representing the linear part of the structure (LS) and a bearing representing the nonlinear part of the structure (CSS), was chosen in order to reduce the error in modelling the linear substructure as low as possible. This way the CSS model has the greatest influence on how the experimental and analytical results of the connected structure correlate.

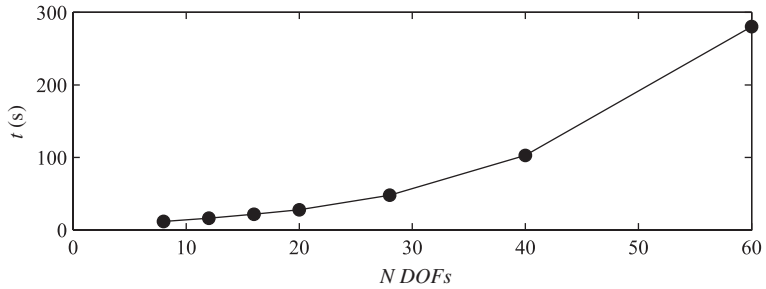

Fig. 9. The exponential growth of the nonlinear-FRF calculation time with respect to the number of dofs retained for the case of the beam structure from Fig. 7.

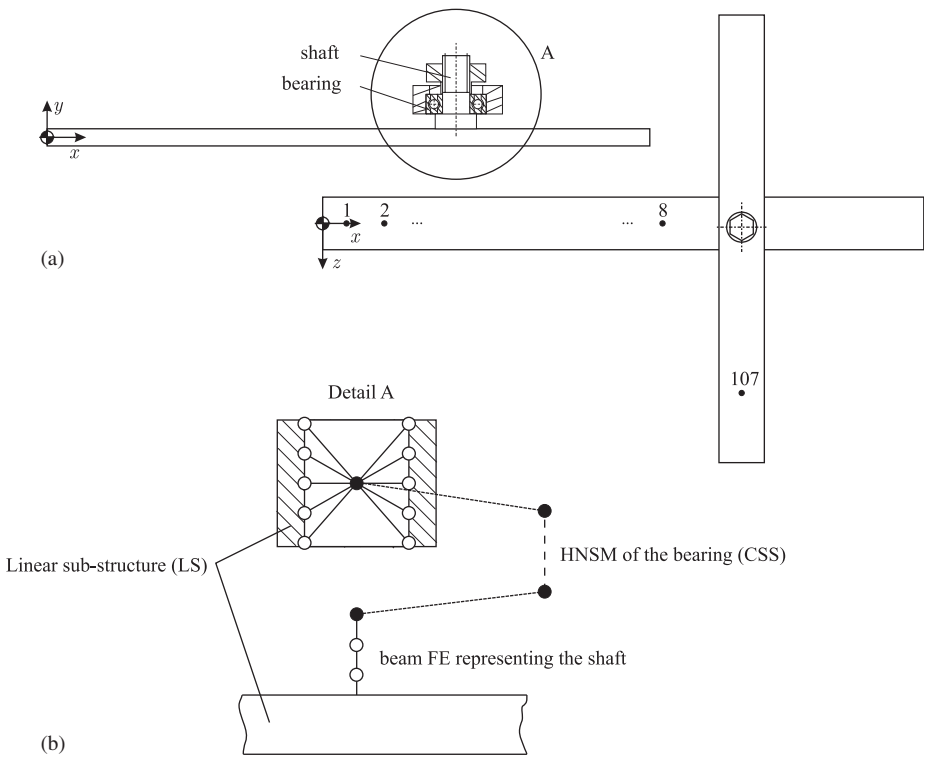

Fig. 10. A T-structure connected by two beams and a typical CSS system, a deep-groove ball bearing (a); the detail at the coupling region shows the linear part of the structure and the CSS model of the bearing in a de-coupled state (b).

The two beams were modelled and updated in the linear domain using a FE package. The response model for each of the two beams was obtained by a modal synthesis using 60 modes; e.g., for the p,q dofs, the accelerance using the hysteretic and proportional damping model, $H_{A_{pq}}$, is [16]

$$H_{A_{pq}}(\omega) = -\omega^2 \sum_{r=1}^{m} \frac{\phi_{pr}\phi_{qr}}{\omega_r^2 - \omega^2 + \mathrm{i}\eta_r\omega_r^2} \tag{35}$$

with the modal damping η_r identified with Ewins–Gleeson's EMA method, with the terms from the modal matrix ϕ_{pr} and undamped natural frequencies ω_r obtained using the linear finite-element software. This corresponds to the top part of the algorithm in Fig. 1.

The detailed, nonlinear CSS model for the bearing (see the corresponding blocks in Fig. 1), used for the determination of the coefficients for the internal-force approximation, was a 6-dof nonlinear model from [17] and further expanded to a 12-dof model [18], as shown in Fig. 11(a). The internal-force approximation, using the linear and cubic terms, was the same as in the case of the joint between the beams from Section 4.2

$$\hat{f}_k = \hat{f}_k(\mathbf{x}) = \sum_{j=1}^{n} a_{k_j}x_j + \sum_{j=1}^{n} b_{k_j}x_j^3 + \sum_{j=1}^{n-1}\sum_{i=j+1}^{n} c_{k_{j,i}}x_j^2x_i + \sum_{j=1}^{n-1}\sum_{i=j+1}^{n} d_{k_{j,i}}x_jx_i^2 \tag{36}$$

the result of which is shown in Fig. 11(b) for the example of an x and y displacement-dependent internal force in the y direction. The HNSM model for the bearing (the middle part of the algorithm from Fig. 1) was obtained in the same way as in Section 4.2. FRF coupling from Eq. (1) was used to couple two LSs, the two beams, with the CSS model, the HNSM of the bearing—note the corresponding block in Fig. 1.

Fig. 12 shows two experimental FRFs on the T-structure [15] obtained using random excitation at two different RMS values of the excitation force. Thus obtained FRFs are so-called linearized FRFs that cannot show nonlinear phenomena. On the same graphs there are also numerically obtained nonlinear FRFs using coupling and the HNSM approach proposed, but under the constant excitation force-amplitude over the whole frequency band of interest—these are nonlinear FRFs that can show the nonlinear phenomena, e.g., jump phenomena. In the frequency band of the first two resonances the numerical prediction is quite satisfactory, even in terms of amplitudes and not only in terms of resonance locations.

In order to investigate any possible nonlinear phenomena experimentally and to compare directly to the numerical results, the T-structure was also tested using sine excitation with a constant amplitude of the force. Fig. 13 shows three experimental accelerance FRFs [15] with the corresponding numerical FRFs where the overall agreement, shown around the first resonance area, is again satisfactory up to 300 Hz, in the bandwidth of the first two resonances. The experimental results from Fig. 13, especially the FRFs for the force of 6 and 10 N, apparently did not exhibit the same nonlinear behaviour as the corresponding numerical FRFs. The reason is, that, although a special-purpose measurement hardware was used (hardware loop-control) with the aim to provide a constant force on the input, at the input force of 6 and 10 N the hardware did not succeed to maintain the force level constant around resonances.

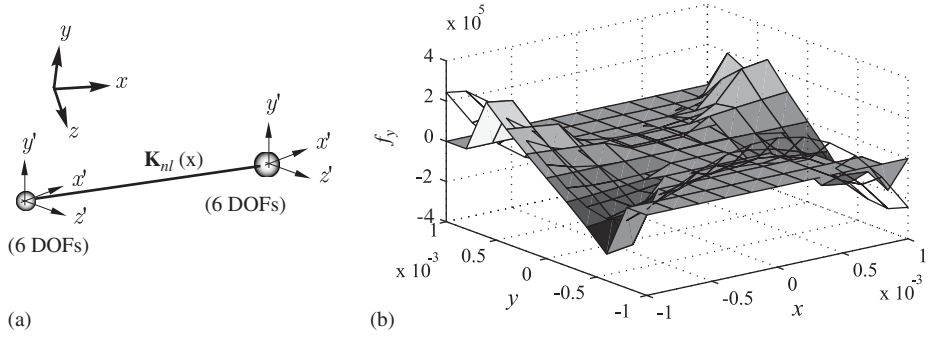

Fig. 11. The 12-dof bearing model [17,18] (a); the exact (filled surface) and the approximate (mesh) internal force–displacement relation for the bearing's HNSM model (b).

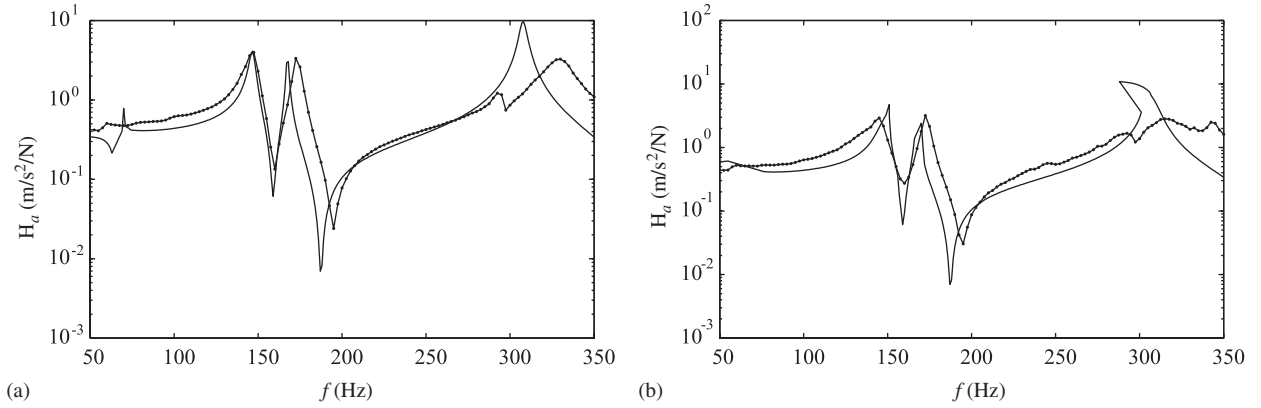

Fig. 12. Experimental accelerance FRFs (-.-) with the random excitation and the numerical FRFs (—) with the constant force for the 107—2, 8—2 coordinate pair. Amplitude and/or RMS level of the force was 1 N (a) and 6 N (b).

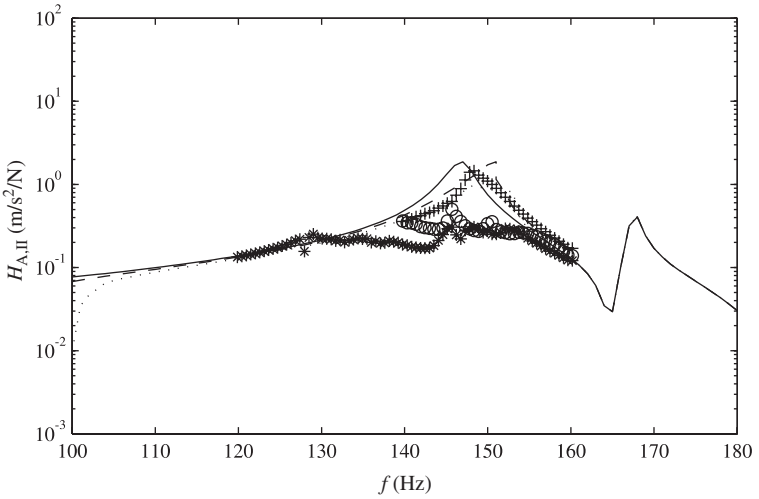

Fig. 13. The experimental and numerical accelerance FRFs for three levels of the excitation force around the first resonance: the experimental FRFs are shown at forces of 1 N (+), 6 N (o) and 10 N (*); the numerical FRFs are shown at forces of 1 N (–), 6 N (- -) and 10 N (...). In all cases the excitation force was constant.

The not-so-good agreement between the experimental and the numerical FRFs in the frequency band from 300 Hz and above is a result of the simple model of the bearing and, most probably, due to the modelling simplification of the connection between the bearing's outer ring and the beam that was assumed to be rigid; i.e., in the bearing, only the balls were assumed being elastic.

6. Conclusions

The proposed approach of building the HNSM for a steady-state vibration analysis of CSs proves to be valid with respect to a direct approach using numerical integration or even with respect to the classical describing-function approach using inter-coordinate notation (where applicable, e.g., in this paper shown for the cubic nonlinearity and the clearance of a 2-dof system). Also, this approach can be enhanced to account for higher harmonics. Eventually, this approach (the HNSM) enables us to build a model of a CSS in the form of the linear and nonlinear parts which means that a choice of whether a nonlinear part can be neglected or not can easily be made. This can be done by simply performing a preliminary analysis with and without the nonlinear part. The latter would not be possible in the case of the harmonic balance approach for example. The harmonic balance approach also needs additional iteration, which makes this approach less efficient than

in the case of the describing functions. Moreover, the reduction of the linear and nonlinear parts, together with the expansion, speeds up the calculation considerably, while the accuracy of the results is preserved if a sufficient number of master coordinates is retained.

Experimental results on a special-purpose T-structure showed that the proposed approach of incorporating localised nonlinearities in the form of the HNSM can be used to predict the nonlinear FRFs of real structures having such nonlinear elements, in terms of resonances as well as in terms of amplitudes. Due to simplifications in the modelling of the bearing and due to the reduction and the two-stage approximation in the process of building the HNSM, the experimental results were satisfactory around the first two resonances. Further work on different types of CSS systems, on use of different detailed CSS models as well as different HNSM models is still required in order to be able to draw additional conclusions on the use of the HNSM proposed.

Acknowledgements

This research was supported by the Ministry of Higher Education, Science and Technology of the Republic of Slovenia.

References

[1] D.J. Ewins, D.J. Inman, *Structural Dynamics @ 2000: Current Status and Future Directions*, Research Studies Press Ltd., Baldock, Hertfordshire, England, 2001.
[2] E. Dascotte, R. Swindell, Beyond modal animations: modal pre-test planning, structural dynamics modifications & integration with fea, *Modal Analysis and Lab Test Simulation Seminar*, m + p International, UK, 2003.
[3] W. Liu, Structural Dynamic Analysis and Testing of Coupled Structures, PhD Thesis, Imperial College of Science, Technology and Medicine, University of London, 2000.
[4] D.W. Fotsch, Development of Valid FE Models for Structural Dynamic Design, PhD Thesis, Imperial College of Science, Technology and Medicine, University of London, 2001.
[5] W.L. Li, A new method for structural model updating and joint stiffness identification, *Mechanical Systems and Signal Processing* 16 (1) (2002) 155–167.
[6] J.E. Mottershead, M.I. Friswell, Model updating of joints and connections, *International Conference on Structural Dynamics Modelling*, 2002.
[7] L. Gaul, J. Lenz, Nonlinear dynamics of structures assembled by bolted joints, *Acta Mechanica* 125 (1–4) (1997) 169–181.
[8] K.Y. Saniturk, M. Imregun, D.J. Ewins, Harmonic balance vibration analysis of turbine blades with friction dampers, *Journal of Vibration and Acoustics-Transactions of the ASME* 119 (1) (1997) 96–103.
[9] J.V. Ferreira, Dynamic Response Analysis of Structures with Nonlinear Components, PhD Thesis, Imperial College of Science, Technology and Medicine, University of London, 1998.
[10] G. von Groll, D.J. Ewins, The harmonic balance method with arc-length continuation in rotor/stator contact problems, *Journal of Sound and Vibration* 241 (2) (2001) 223–233.
[11] J.V. Ferreira, A.L. Serpa, Application of the arc-length method in nonlinear frequency response, *Proceedings of the International Modal Analysis Conference—IMAC*, SEM, Bethel, CT, USA, 2002.
[12] M.I. Friswell, J.E.T. Penny, S.D. Garvey, Using linear-model reduction to investigate the dynamics of structures with local nonlinearities, *Mechanical Systems and Signal Processing* 9 (3) (1995) 317–328.
[13] S. Meyer, M. Link, Modelling and updating of local non-linearities using frequency response residuals, *Mechanical Systems and Signal Processing* 17 (1) (2003) 219–226.
[14] W. Liu, D.J. Ewins, Substructure synthesis via elastic media—part i: joint identification, *Proceedings of the International Modal Analysis Conference—IMAC*, SEM, Bethel, CT, USA, 2000.
[15] P. Čermelj, Dynamics of Complex Structures with Localised Nonlinearities, PhD Thesis, Faculty of Mechanical Engineering, University of Ljubljana, 2005.
[16] D.J. Ewins, *Modal Testing: Theory and Practice*, Research Studies Press Ltd., Wiley, New York, Brisbane, Chichester, Toronto, Singapore, 1986.
[17] T.C. Lim, R. Singh, Vibration transmission through rolling element bearings—1: bearing stiffness formulation, *Journal of Sound and Vibration* 139 (2) (1990) 179–199.
[18] P. Čermelj, M. Boltežar, An indirect approach to investigating the dynamics of a structure containing ball bearings, *Journal of Sound and Vibration* 276 (1–2) (2004) 401–417.